JOURNAL OF THE
CHUNGCHEONG MATHEMATICAL SOCIETY
Volume **20**, No. 4, December 2007

PARAMETRIC INVESTIGATIONS ON THE DOUBLE DIFFUSIVE CONVECTION IN TRIANGULAR CAVITY

SunJoo Kwon*, SeYoung Oh**, Jae Heon Yun***,
and Sei-Young Chung****

Abstract. Double-diffusive convection inside a triangular porous cavity is studied numerically. Galerkin finite element method is adopted to derive the discrete form of the governing differential equations. The first-order backward Euler scheme is used for temporal discretization with the second-order Adams-Bashforth scheme for the convection terms in the energy and species conservation equations. The Boussinesq-Oberbeck approximation is used to calculate the density dependence on the temperature and concentration fields. A parametric study is performed with the Lewis number, the Rayleigh number, the buoyancy ratio, and the shape of the triangle. The effect of gravity orientation is considered also. Results obtained include the flow, temperature, and concentration fields. The differences induced by varying physical parameters are analyzed and discussed. It is found that the heat transfer rate is sensitive to the shape of the triangles. For the given geometries, buoyancy ratio and Rayleigh numbers are the dominating parameters controlling the heat transfer.

1. Introduction

In the past two decades, there were numerous attempts to study double-diffusive phenomena owing to its wide encounters in the nature and vast engineering applications [1]. Specially, the double-diffusive phenomenon in an enclosure is considered as an important research area in fluid engineering because of its promising application in the manufacturing, Differences in the molecular thermal and mass diffusivities of the fluids make the double-diffusive convection phenomena unique from

Received September 30, 2007.
2000 Mathematics Subject Classification: Primary 65M60 76E06.
Key words and phrases: double diffusive convection, triangular cavity, Boussinesq-Oberbeck approximation, Galerkin method.

ordinary convective phenomena. Majority of both experimental and theoretical approaches on the double-diffusive convection is confined to a rectangular geometry where emphasis were given to the basic feature of the convection effects. There are several attempts on studying the double-diffusive phenomena in different geometries. Different geometries such as spheres and cylinders are succinctly reviewed for the double-diffusive convection in porous media[2]. Thus far, literatures on the double-diffusive convection are ample, however, there are very few literatures addressing the double-diffusive convection in triangle geometry even though its possible wide applications in the engineering problems. The purpose of our present study is to investigate the double-diffusive phenomena in triangular geometries.

There are several reported studies on the flow in a trapezoidal cavity which is close to the triangular geometry. Separated flow in a trapezoidal driven cavity is studied by Darr and Vanka[3]. Interesting flow pattern owing to the trapezoidal geometry is reported in their study. Double-diffusive convection phenomena in the anisotropic trapezoidal porous cavity is studied by Nguyen et al.[4]. They reported different number of the separated flow loops in the cavity where the number of the loops was depending on the geometric configuration as well as the dimensionless groups of the flow.

Even though most of the literature on the double-diffusive convection are in the rectangular or trapezoidal geometries, the triangular cavity can be encountered in the corrugated components of pipes or ducts and at least as common in practice as the square[5]. Despite of the wide encounters in the engineering problems, it is a very recent effort that Ribbon et al. [6] investigate the viscous flow characteristics in the triangular cavity. In their study, numerical assessment results are shown for the unique viscous flow characteristics in the triangular cavity by using finite difference formulation, The numerical treatment of the singular points of the triangle was the major concern of their study. So far, to our knowledge, the double-diffusive convection in a triangular cavity has not been addressed by any researchers.

The purpose of this study is parametric investigation on the double-diffusive convection in triangular cavities. Three different types of triangle cavity shapes are considered in order to show the geometric effects on the double-diffusive convection. The Boussinesq-Oberbeck approximation for the density dependence on the temperature and the concentration is used to account for the buoyancy force induced by temperature and concentration fields. The governing equations are based on

the mass, momentum, and energy conservation laws. The nondimensionalizing parameters are selected for the dependent variables in the governing equations. The nondimensional form of the governing equations are presented and solved in the triangular meshes. Galerkin finite element method is used in order to avoid the special treatments on the triangular shape in the finite difference method[6].

2. Problem description and mathematical formulation

Triangular enclosure considered in this study is shown in Figure 1 which is filled with an porous material. The porous material is saturated with a binary fluid which is initially at uniform temperature T_0 and uniform concentration S_0. At time $t = 0$, the left side wall is exposed to different temperature T_1 and concentration S_1. The right side wall is subjected to a constant temperature T_0 and concentration S_0 fields throughout the simulation time. The bottom wall is kept insulated to the heat and mass penetration. Under gravitational field, the imposed temperature arid concentration differences cause local density differences and induce the fluid movement. The coupled effects of the temperature and concentration gradients on the transports inside the cavity can be described by using a set of governing equations. In this study, local thermal equilibrium with negligible dispersion is assumed. Soret and Dufour effects are neglected. By assuming the fluid is obeying the Darcy's law the mass, momentum, and energy conservation equations can be written as follows:

$$\boldsymbol{\nabla}\cdot\mathbf{u} = \mathbf{0} \tag{2.1}$$

$$\mathbf{u} = -\frac{\mathbf{K}}{\mu}\left[\boldsymbol{\nabla}p - \rho_f g\mathbf{j}\right] \tag{2.2}$$

$$\left[\phi(\rho c)_f + (1-\phi)(\rho c)_s\right]\frac{\partial T}{\partial t} + (\rho c)_f \mathbf{u}\cdot\boldsymbol{\nabla}T = \kappa\boldsymbol{\nabla}^2 T \tag{2.3}$$

$$\phi\frac{\partial S}{\partial t} + \mathbf{u}\cdot\boldsymbol{\nabla}S = D\boldsymbol{\nabla}^2 S \tag{2.4}$$

where $\mathbf{u}$ is the Darcian velocity vector, p is the pressure, t is the time, $\mathbf{K}$ is the permeability tensor, g is the gravity. κ is the effective thermal conductivity. μ is the viscosity, c is the heat capacity, ρ is the density, ϕ is the porosity. The subscripts f and s denote the fluid and solid phases respectively.

In order to avoid difficulties arising from specifying boundary conditions for the pressure, we adopt the stream-function formulation in this study. The stream-function(Ψ) is defined by using the velocity as

$$\mathbf{u} = \frac{\partial \Psi}{\partial y}\mathbf{i} - \frac{\partial \Psi}{\partial x}\mathbf{j} \tag{2.5}$$

where $\mathbf{i}$ and $\mathbf{j}$ are the unit vectors in $x-$ and $y-$ directions, respectively. In order to perform parametric study, the governing equations are recasted in the dimensionless form. The variables are nondimensionalized by using the following dimensionless parameters:

$$t^* = \frac{\alpha t}{L_b^2}\ ,\ (x^*, y^*) = \frac{(x, y)}{L_b}\ ,\ \Psi^* = \frac{\Psi}{\alpha},$$

$$S^* = \frac{S - S_0}{S_1 - S_0}\ ,\ T^* = \frac{T - T_0}{T_1 - T_0}\ ,\ B = \frac{\beta_s(S_1 - S_0)}{\beta_T(T_1 - T_0)},$$

$$\sigma = \frac{\phi(\rho c)_f + (1-\phi)(\rho c)_s}{(\rho c)_f},$$

$$Ra = \frac{K\beta_s g L_b(T_1 - T_0)}{\alpha \upsilon}\ ,\ Le = \frac{\alpha}{D}. \tag{2.6}$$

α and υ are the thermal diffusivity and kinematic viscosity respectively. The asterisks are representing the variable is in dimensionless form. From now on, the asterisks will be omitted for the convenience. Ra, Le, and B are the Rayleigh number, Lewis number and the buoyancy ratio in respective order. L_b denotes the bottom length of a triangle. Since the present study only focuses on the isotropic porous media, the scalar K represent the permeability tensor at every location inside the triangular region.

Following the study in anisotropic porous media by Nguyen et al.[4], we adopted the Boussinesq-Oberbeck approximations which can be written as

$$\rho_f = \rho_0 \left[1 - \beta_T(T - T_0) + \beta_s(S - S_0)\right]. \tag{2.7}$$

Equation (7) states that the density is proportional bilinearly to the temperature and concentration changes.

By utilizing the above equations(5, 6, 7), the governing equations can be recanted in the dimensionless form as :

$$\left(\frac{\partial}{\partial x} + \frac{\partial}{\partial y}\right)\left(\frac{\partial \Psi}{\partial x} + \frac{\partial \Psi}{\partial y}\right) = -Ra\left[\frac{\partial T}{\partial x} - B\frac{\partial S}{\partial x}\right] \tag{2.8}$$

$$\sigma\frac{\partial T}{\partial t} - J(\Psi, T) = \frac{\partial^2 T}{\partial x^2} + \frac{\partial^2 T}{\partial y^2} \tag{2.9}$$

$$\phi\frac{\partial S}{\partial t} - J(\Psi, S) = \frac{1}{L_e}\left[\frac{\partial^2 S}{\partial x^2} + \frac{\partial^2 S}{\partial y^2}\right] \tag{2.10}$$

where $J(,)$ represents the Jacobian. Because of the Darcian flow assumption used in this study, the inertia and the boundary effects on the momentum transfer are neglected. Thus the present analysis is restricted to creeping-like-flow in low porosity media.

3. Numerical procedure

Following the earlier work of Nguyen et al. [4], we adopt semi-implicit procedure which combines the second-order Adams Bashforth and the first-order backward Euler schemes for time integration. Discretization with the time derivative terms by using the combination of the first order implicit and second order explicit schemes yields the governing equations in the form as follows:

$$\begin{aligned}\left[\frac{\sigma}{\Delta t} - \left(\frac{\partial^2}{\partial x^2} + \frac{\partial^2}{\partial y^2}\right)\right] T^{n+1} \\ = \frac{\sigma}{\Delta t}T^n + \frac{1}{2}\left[3J(\Psi^n, T^n) - J(\Psi^{n-1}, T^{n-1})\right]\end{aligned} \tag{3.1}$$

$$\begin{aligned}\left[\frac{\phi}{\Delta t} - \frac{1}{L_e}\left(\frac{\partial^2}{\partial x^2} + \frac{\partial^2}{\partial y^2}\right)\right] S^{n+1} \\ = \frac{\phi}{\Delta t}S^n + \frac{1}{2}\left[3J(\Psi^n, S^n) - J(\Psi^{n-1}, S^{n-1})\right]\end{aligned} \tag{3.2}$$

$$\left(\frac{\partial}{\partial x} + \frac{\partial}{\partial y}\right)\left(\frac{\partial \Psi^{n+1}}{\partial x} + \frac{\partial \Psi^{n+1}}{\partial y}\right) = -Ra\left[\frac{\partial T^{n+1}}{\partial x} - B\frac{\partial S^{n+1}}{\partial x}\right] \tag{3.3}$$

where Δt is the time increment and the superscripts $n+1$, n, and $n-1$ represent the new, current and old time levels. Since the temperature and concentration fields are updated by Adams-Bashforth scheme, the flow field is solved after the new time solutions for the temperature and concentration fields are obtained.

Galerkin finite element method is used to spatially discretize the governing equations. In the finite element method, the calculation domain is subdivided into number of sub-domain element. For every element,

the dependent variable is expanded with a set of basis functions multiplied by the representing coefficients. The details of the Galerkin finite element procedure can be found elsewhere[7]. Thus the details of the method will be omitted in this paper. By using the principal of weighted residual with the Galerkin procedure, the resulting discretized equations can be written as follows :

$$\sum_{e=1}^{NE}[A_T]^e\{T\}^e = \sum_{e=1}^{NE}\{b_T\}^e, \tag{3.4}$$

$$\sum_{e=1}^{NE}[A_S]^e\{S\}^e = \sum_{e=1}^{NE}\{b_S\}^e, \tag{3.5}$$

$$\sum_{e=1}^{NE}[A_\Psi]^e\{\Psi\}^e = \sum_{e=1}^{NE}\{b_\Psi\}^e, \tag{3.6}$$

where NE is the total number of elements. $[A_T]^e$, $[A_S]^e$, and $[A_\Psi]^e$ are the element matrices and $\{b_T\}^e$, $\{b_S\}^e$, and $\{b_\Psi\}^e$ are the known right-hand-side vectors.

4. Results and discussions

The numerics used in this study are similar to those used for the non-rectangular enclosure double-diffusive convection[4]. Thus, the verification of the present numerics is revered to [4]. Since our main purpose of this study is to explore the effect of triangular geometry on the double-diffusive convection phenomena, we will focus our attention on three equilateral triangles with bottom length $L_b = 1$ and its side angles $\beta = 0.15\pi,\ 0.33\pi$, and 0.45π. Three different β values are used to examine the geometric effects. The boundary conditions are specified as to allow no heat and mass are penetrated along the bottom wall and temperature and concentration differences are imposed across the left to right walls. Thus, the mathematical representation for the boundary conditions can be written as

$$T = 1 \text{ along } \partial\Omega_l\ ,\ T = 0 \text{ along } \partial\Omega_r\ ,\ \mathbf{n}\cdot\boldsymbol{\nabla}T = 0 \text{ along } \partial\Omega_b\ ,$$

$$S = 1 \text{ along } \partial\Omega_l\ ,\ S = 0 \text{ along } \partial\Omega_r\ ,\ \mathbf{n}\cdot\boldsymbol{\nabla}S = 0 \text{ along } \partial\Omega_b\ ,$$

where the subscripts l, r, and b denote the left, right, and bottom walls in respective order.

In order to study the effects of Lewis and Rayleigh numbers, calculations are made for the different Lewis number, buoyancy ratio, and Rayleigh number The steady state concentration, flow, and temperature fields for $Le = 1$, $B = 0$, and $Ra = 10$ case are shown for the three different geometries in Figure 1. The steady state is assumed to be reached if the following criteria are reached:

$$\frac{\left|Z^{n+1} - Z^n\right|}{|Z^n|} \leq \epsilon \tag{4.1}$$

where Z represents dependent variables and superscript n and $n + 1$ represent the time levels. The tolerance ε is set to be 10^{-3}. Owing to the small Lewis number, the concentration fields show near to symmetric profiles along the geometric centerline in Figure 1. However, the temperature fields show the slightly concentrated isotherms toward the high temperature wall. Both the concentration and temperature profiles show iso-lines perpendicular to the bottom wall because of the no flux boundary condition adopted in this study. The buoyancy induced flow in the triangles show more mass flux near the walls compared to the center since the temperature differences are specified along the wall without any internal heat sources.

In order to demonstrate the effect of direction of gravity, the results of opposite gravity case for $Le = 1$ and $Ra = 100$ case is shown in Figure 2. is distorted near that surface for the opposite gravity.

For the case of high Lewis number, Figure 3 shows the results for the $Le = 10$, $B = 0$, and $Ra = 100$ case with $\beta = 0.45\pi$. The concentration fields shows the higher concentration fields penetrate to the cold wall side along the wall. Since it is assumed that the mass transfer does not contribute to heat transfer, the isotherm contours show no difference from the one obtained for $Le = 1$ and $Ra = 100$ case. However, it is noticeable that the mass is transported by the convection current more efficiently in case of high Lewis number case. As a result, the iso-concentration lines shows sharp edges along the convected current.

Figure 4 shows the case for $B = 1$, $Le = 5$, and $Ra = 200$. Here the flow fields show multi-cell flow patterns. The Boussinesq-Oberbeck approximation adopted in this study implies that for $B = 1$, the density changes due to the concentration changes are about the same magnitude changes due to the temperature changes. The corresponding effects on the buoyancy force due to the concentration changes are significant for

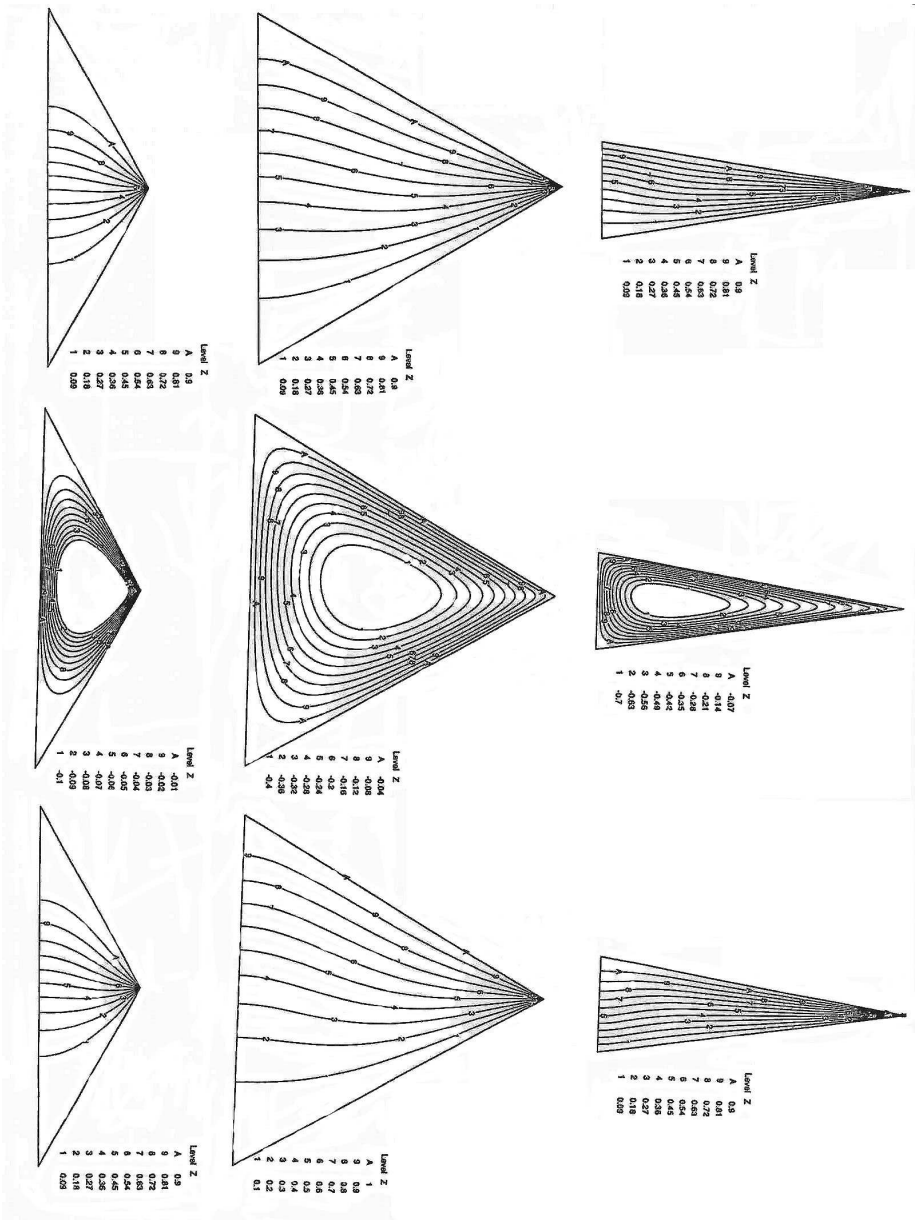

FIGURE 1. Steady state solution of concentration(left), flow(middle), and temperature(right) fields for $L_e = 1, B = 0$, and $R_a = 10$ case with gravity downward direction.

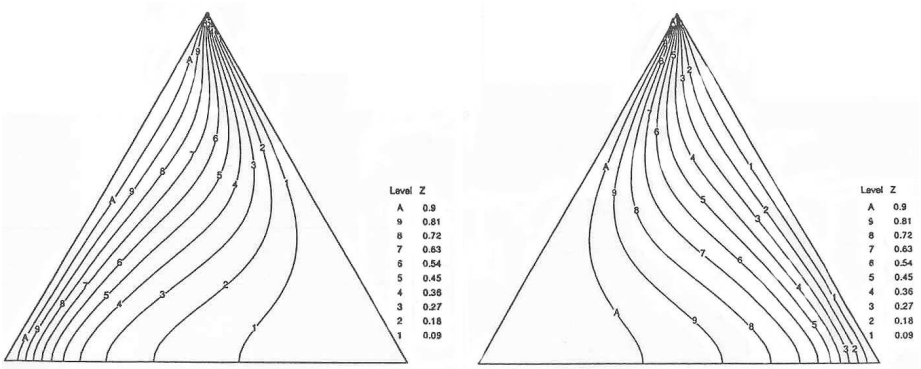

FIGURE 2. The mirror images of distortions of concentration field for gravity downward direction(left) and gravity upward direction(right) with $L_e = 1, B = 0$, $R_a = 100$, and $\beta = 0.33\pi$.

$B = 1$ and as a results the flow fields show the multiple recirculating cells. It is also interesting the shape of the recirculating cells changes for different β cases. For $\beta = 0.15\pi$ case, there are three recirculating loops in the streamline contours. The strongest recirculation occurs near the top of the triangle and the second and the third ones occurs along the left wall boundaries. The corresponding concentration field show more distorted iso-concentration lines near the top of the triangle. For the $\beta = 0.33\pi$, there are two cells in the flow field. In this case, the strongest recirculation occurs along the hot wall and extends the flow almost the half of the cold wall. There is significant effects on the concentration fields due to the strong recirculation where one can find the concentration plateau near the hot wall. The second recirculation is very weak and shows very little effects on both the concentration and temperature profiles. Thus the temperature fields near the secondary recirculation zone show almost uniform temperature profiles. In the case of $\beta = 0.45\pi$, there are two recirculation zone formed with approximately same magnitude. The stronger recirculation zone is found near the left wall corner which is contrast to the case of $\beta = 0.15\pi$ case. The corresponding temperature fields show that the steepest temperature gradient can be found at the left side corner because the cold fluids are pushed to the side by the strong convection. The similar trends can be found for the concentration fields. It is noteworthy that the effects of different triangle shape can results in different flow, concentration,

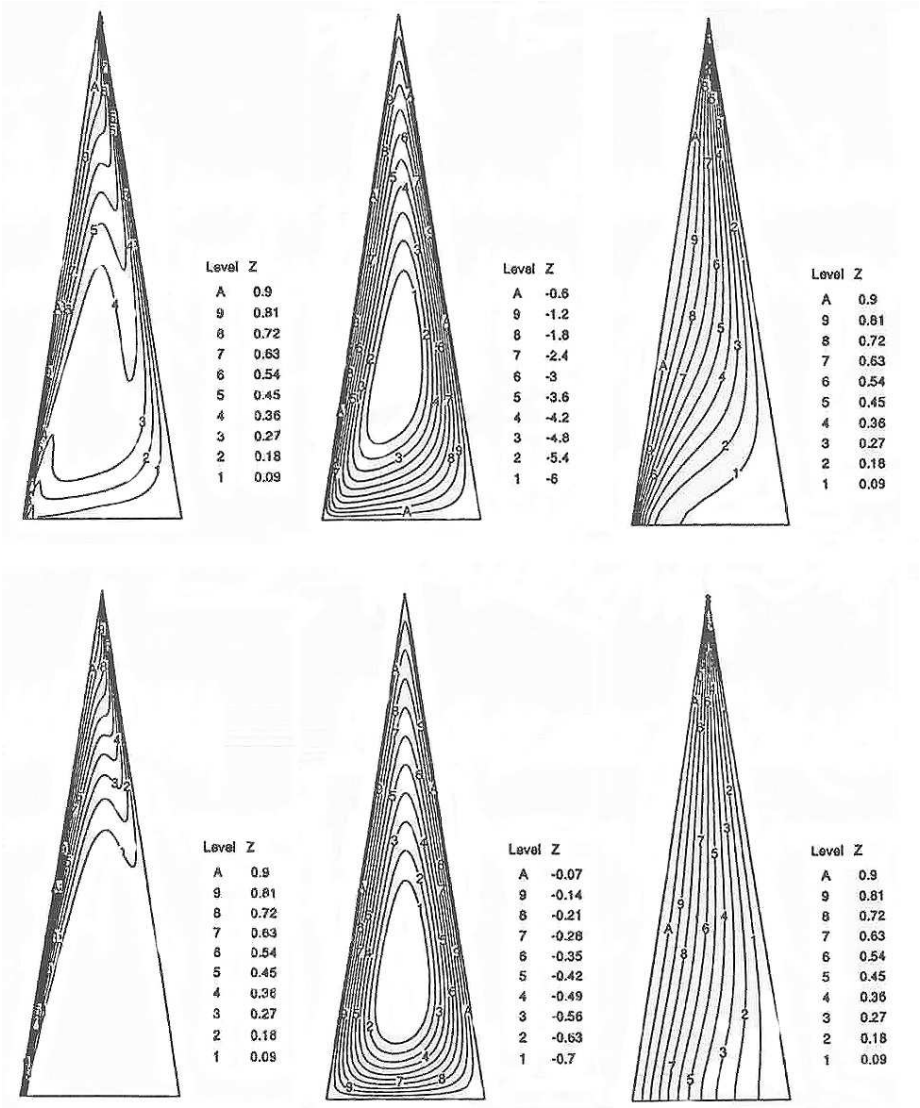

FIGURE 3. Steady state solution of concentration(left), flow(middle), and temperature(right) fields for $L_e = 10, B = 0$, and $R_a = 100$ case(top) and $L_e = 100, B = 0$, and $R_a = 10$ case(bottom)with gravity downward direction.

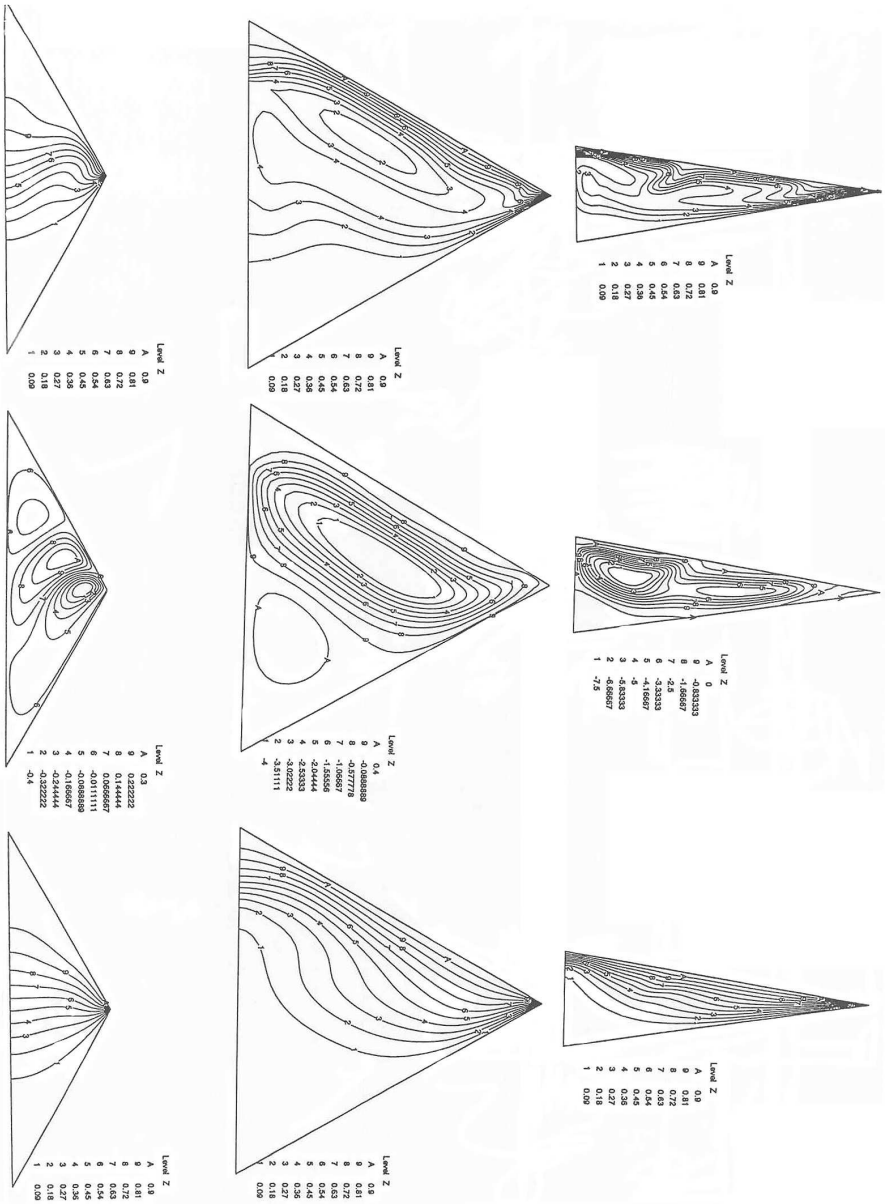

FIGURE 4. Steady state solution of concentration(left), flow(middle), and temperature(right) fields for $L_e = 5, B = 1$, and $R_a = 200$ case with gravity downward direction.

and temperature fields. The number of the cells and magnitude of the recirculations are also significantly affected by the geometries.

For the higher $B = 3$ with the same Le and Ra numbers, the multi-cell flow patterns were no longer found. Instead, the flow fields show that strong convection is found along the side walls. Relatively, the core of the triangles are not affected by the convection, resulting relatively straight iso-concentration and isotherm lines near the centers. It is interesting to note that the steeper concentration and temperature fields are found near the cold wall corner in this case.

In order to investigate the effects of various parameters on the heat transfer, Nusselt number is selected as an indicator for the heat transfer rate. The Nusselt number in this study is defined as

$$Nu \equiv \frac{q}{\kappa(T_1 - T_0)/L_b} = \int_{L_e} \frac{\partial T}{\partial x}(\partial\Omega_e)dy \tag{4.2}$$

where q is the total heat transfer rate. The calculated Nusselt number for the selected cases are shown in Figure 5. In order to illustrate the effects of different Rayleigh number, the Nusselt numbers are plotted on the top of Figure 5. For the same geometrical and physical parameters, the high Rayleigh number results in the heat transfer rate is high as one can expect. It should be mentioned here that the different β angles effects on the heat transfer are significant. As the β angle increases, the heat transfer rate increases order of magnitude. This is parity owing to the definition of the Nusselt number we used in this study. The Nusselt number is defined by using the length of the bottom wall as the characteristic length. However, it is depicted in the isotherms that the temperature contours have steeper gradients as the β angle increases.

The effects of the B ratio on the heat transfer rates are illustrated in the middle of Figure 5. In general, it can be said that as the B ratio increases, the heat transfer rate decreases. However, for the case that the multi-cell convection is dominant, the Nusselt number has oscillatory behavior with a long wavelength as shown in the graphs. The bottom of Figure 5 shows the effects of the gravitational direction on the heat transfer rate and the fact that the gravity direction does not affect the heat transfer rate significantly. It is due to the mirror image of the temperature fields calculated for the positive and negative gravity directions.

The study on the trapezoidal geometry by Nguyen et al.[4] shows that the different Lewis number does not affect the heat transfer rate significantly. Thus, parametric study on the effect of Lewis number on the triangle geometry is omitted in this study.

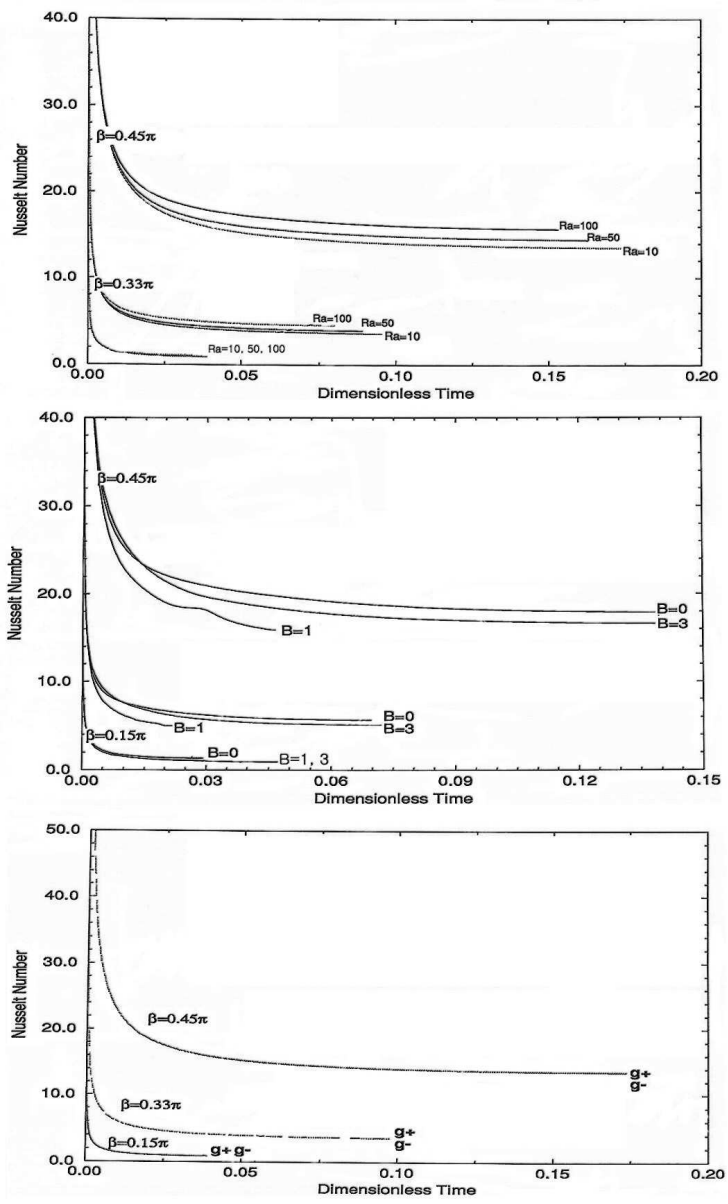

FIGURE 5. Transient Nusselt number for different R_a number(top), different B(middle), and different gavity directions(bottom).

References

[1] C. F. Chen and D. H. Johnson, *Double-diffusive convection: A report on an engineering foundation conference*, J. Fluid Mech. Digital Archive **138** (1984) 405-416.
[2] D. A. Nield and A. Bejan, *Convection in porous media*, Springer-Verlag, New York, 2006.
[3] J. H. Darr and S. P. Vanka, *Separated flow in a driven trapezoidal cavity,* Phys. Fluids A. **3** (1991), no. 3, 385-392.
[4] H. D. Nguyen, S. Paik, and R. W Douglass, *Double-diffusive convection in a non-rectangular enclosure filled with an anisotropic porous medium having blique principal axes*, private communication, (2002).
[5] E. M. Sparrow and M. Charmchi, *Heat transfer and fluid flow characteristics of spanwise-periodic corrugated Ducts*, Int. J. Heat Mass Transfer **23** (1980), 471-481.
[6] C. J. Ribbens, L. T. Watson, and C. Y. Wang, *Steady viscous flow in a triangular cavity* , J. Comp. Phys. **112** (1994), 173-181.
[7] O. C. Zienkiewicz, R. L. Taylor, and J. Z. Zhu, *The finite element method*, Elsevier, 2005.

*
Nuclear Fuel Cycle Strategy Research Lab
Korea Atomic Energy Research Institute
Daejeon 305-353, Republic of Korea
E-mail: sjkw@kaeri.re.kr

**
Department of Mathematics
Chungnam University
Daejeon 305-764, Republic of Korea
E-mail: soh@cnu.ac.kr

***
Department of Mathematics
Chungbuk University
Cheongju 361-763, Republic of Korea
E-mail: gmjae@cbucc.chungbuk.ac.kr

****
Department of Mathematics
Chungnam University
Daejeon 305-764, Republic of Korea
E-mail: sychung@cnu.ac.kr